









## Article

# Drug Metabolism of Hepatocyte-like Organoids and Their Applicability in In Vitro Toxicity Testing

Manon C. Bouwmeester <sup>1</sup>, Yu Tao <sup>1</sup>, Susana Proença <sup>2,3</sup>, Frank G. van Steenbeek <sup>1,4</sup>, Roos-Anne Samsom <sup>1</sup>, Sandra M. Nijmeijer <sup>3</sup>, Theo Sinnige <sup>3</sup>, Luc J. W. van der Laan <sup>5</sup>, Juliette Legler <sup>3</sup>, Kerstin Schneeberger <sup>1</sup>, Nynke I. Kramer <sup>2,3,†</sup> and Bart Spee <sup>1,\*,†</sup>

<sup>1</sup> Department of Clinical Sciences, Faculty of Veterinary Medicine, Regenerative Medicine Center Utrecht, Utrecht University, 3584 CT Utrecht, The Netherlands

<sup>2</sup> Division of Toxicology, Wageningen University, 6700 EA Wageningen, The Netherlands

<sup>3</sup> Institute for Risk Assessment Sciences, Utrecht University, 3584 CM Utrecht, The Netherlands

<sup>4</sup> Department of Cardiology, Division Heart & Lungs, University Medical Center Utrecht, 3508 GA Utrecht, The Netherlands

<sup>5</sup> Department of Surgery, Erasmus MC Transplant Institute, University Medical Center Rotterdam, 3015 CN Rotterdam, The Netherlands

\* Correspondence: b.spee@uu.nl

† These authors contributed equally to this work.

**Abstract:** Emerging advances in the field of in vitro toxicity testing attempt to meet the need for reliable human-based safety assessment in drug development. Intrahepatic cholangiocyte organoids (ICOs) are described as a donor-derived in vitro model for disease modelling and regenerative medicine. Here, we explored the potential of hepatocyte-like ICOs (HL-ICOs) in in vitro toxicity testing by exploring the expression and activity of genes involved in drug metabolism, a key determinant in drug-induced toxicity, and the exposure of HL-ICOs to well-known hepatotoxicants. The current state of drug metabolism in HL-ICOs showed levels comparable to those of PHHs and HepaRGs for CYP3A4; however, other enzymes, such as CYP2B6 and CYP2D6, were expressed at lower levels. Additionally, EC50 values were determined in HL-ICOs for acetaminophen (24.0–26.8 mM), diclofenac (475.5–>500 μM), perhexiline (9.7–>31.5 μM), troglitazone (23.1–90.8 μM), and valproic acid (>10 mM). Exposure to the hepatotoxicants showed EC50s in HL-ICOs comparable to those in PHHs and HepaRGs; however, for acetaminophen exposure, HL-ICOs were less sensitive. Further elucidation of enzyme and transporter activity in drug metabolism in HL-ICOs and exposure to a more extensive compound set are needed to accurately define the potential of HL-ICOs in in vitro toxicity testing.

**Keywords:** drug-induced liver injury; hepatic in vitro model; hepatotoxicity; intrahepatic cholangiocyte organoids; hepatocyte-like cells



**Citation:** Bouwmeester, M.C.; Tao, Y.; Proença, S.; van Steenbeek, F.G.; Samsom, R.-A.; Nijmeijer, S.M.; Sinnige, T.; van der Laan, L.J.W.; Legler, J.; Schneeberger, K.; et al. Drug Metabolism of Hepatocyte-like Organoids and Their Applicability in In Vitro Toxicity Testing. *Molecules* **2023**, *28*, 621. <https://doi.org/10.3390/molecules28020621>

Academic Editor: Aaron T. Wright

Received: 28 November 2022

Revised: 22 December 2022

Accepted: 5 January 2023

Published: 7 January 2023



**Copyright:** © 2023 by the authors. Licensee MDPI, Basel, Switzerland. This article is an open access article distributed under the terms and conditions of the Creative Commons Attribution (CC BY) license (<https://creativecommons.org/licenses/by/4.0/>).

## 1. Introduction

Drug metabolism is a key determinant in drug-induced toxicity [1]. The liver plays a crucial role in drug metabolism and is, therefore, susceptible to drug-induced injury. Despite the implementation of novel human-based strategies in drug development such as in vitro and in silico pre-clinical testing [2,3], drug-induced liver injury (DILI) remains a major cause for discontinuation of drug development and the withdrawal of drugs from the market [4]. Gaining human-relevant mechanistic insights into DILI is essential to improve toxicity prediction and further minimize adverse drug reactions.

The metabolism of drugs in the liver is generally a two-step process. In phase I, polar functional groups are added or opened up so that phase II enzymes can conjugate the drug to facilitate the drug's excretion. The cytochrome P450 (CYP) superfamily

forms the most prominent and most studied family of phase I biotransformation enzymes [5]. CYP oxidation often leads to bioactivation and is associated with DILI [6]. Genetic polymorphisms in common human CYP isoforms, including CYP2B6, CYP2C9, and CYP2D6, are a common mechanism of adverse drug reactions requiring hospitalization [7,8]. Generally, phase II metabolism by uridine 5'-diphospho-glucuronosyltransferases (UDP-glucuronosyltransferases, UGTs), sulfotransferases (SULTs), and glutathione transferases (GSTs) is a detoxification process, counteracting the reactivity of intermediate metabolites [9]. Hepatic transporters, including superfamilies ATP-binding cassette (ABC) transporters and solute carrier (SLC) transporters, are involved in the excretion of drugs and their conjugated metabolites. Inhibition of efflux transporters leading to intracellular accumulation is another risk factor for drug–drug interaction and DILI [10]. The activities of these two phases of drug metabolism and functionality of hepatic transporters are crucial in hepatotoxicity, as they are responsible for the (de)activation and excretion of chemicals [11,12].

Significant interspecies and interindividual differences in the expression and function of drug metabolism enzymes and transporters hamper accurate prediction of pharmacokinetics in patients and hepatotoxic potency of new drugs, as this is traditionally performed in animal models [13–15]. Over the years, the development of non-animal alternatives evolved to generate human-based toxicity data as well as to replace, reduce and refine animal use (3Rs) in safety evaluations [16,17]. To perform reliable human-based toxicity screens or mechanistic studies into DILI pathways, hepatic human *in vitro* models need to express morphological and functional features, such as drug metabolism, similar to an *in vivo* situation [18].

Human-based hepatic *in vitro* models have been developed using a range of cell sources, where primary human hepatocytes (PHHs), human hepatic cancer cell lines, and human stem cell-derived hepatocyte-like cells are three main hepatic cell sources used in current models [19,20]. In an effort to increase the *in vitro* toxicity prediction by these models, different approaches to enhance the physiological relevance and thereby maintain or improve hepatic function are being developed [21,22]. PHHs are considered the gold standard in *in vitro* toxicity testing, as their phenotype is most comparable to hepatocytes *in vivo*, which can be maintained longer due to advances in the culture method [23]. Besides interspecies differences in drug metabolism that are covered by the use of human-based *in vitro* models, interindividual differences in drug metabolism and thus drug sensitivity are of particular interest [6]. PHHs can represent real human population variability; however, their availability is limited and expansion is very difficult [24–26]. Donor-derived hepatic cell models, such as induced pluripotent stem cells (iPSCs) or adult stem cells (ASCs), can reflect the heterogenous phenotype of the human population and have the potential to be expanded for high-throughput purposes [27].

Human intrahepatic cholangiocyte organoids (ICOs) are liver-derived ASCs that form hollow polarized 3D structures *in vitro* and, once differentiated towards the hepatic lineage, show an increased expression of hepatic markers such as albumin, CYP enzymes, and transporters [28]. The applicability of these hepatocyte-like ICOs (HL-ICOs) for disease modelling and regenerative medicine has been described [29–33]; however, the potential of HL-ICOs as a novel cell model for DILI still needs to be explored [34]. Here, we sought to explore the potential of HL-ICOs for *in vitro* toxicity testing compared to PHHs and the tumor-derived hepatic cell line HepaRG. We focused on the expression of genes involved in phase I and II drug metabolism and hepatic transporters and phase I enzyme and UGT activity. Additionally, we tested a set of known hepatotoxic compounds, namely acetaminophen, diclofenac, perhexiline, troglitazone, and valproic acid, to study cytotoxicity after exposure.

## 2. Results

Intrahepatic cholangiocyte organoids (ICOs) were cultured in conventional Matrigel droplets and differentiated towards the hepatic lineage. After differentiation, hepatocyte-like ICOs (HL-ICOs) formed polarized 3D structures with a hollow lumen with a submembranous positivity for F-actin (Figure 1). The hepatic differentiation status of HL-ICOs indicated an increase in hepatic markers including albumin and CYP3A4 (Supplemental Figure S1), comparable to previous studies [28,31,35]. The hepatic cell line HepaRG was cultured in standard 2D monolayer, and PHHs were cultured as monolayer in a collagen I sandwich (Figure 1), both with an F-actin located on intercellular filaments.

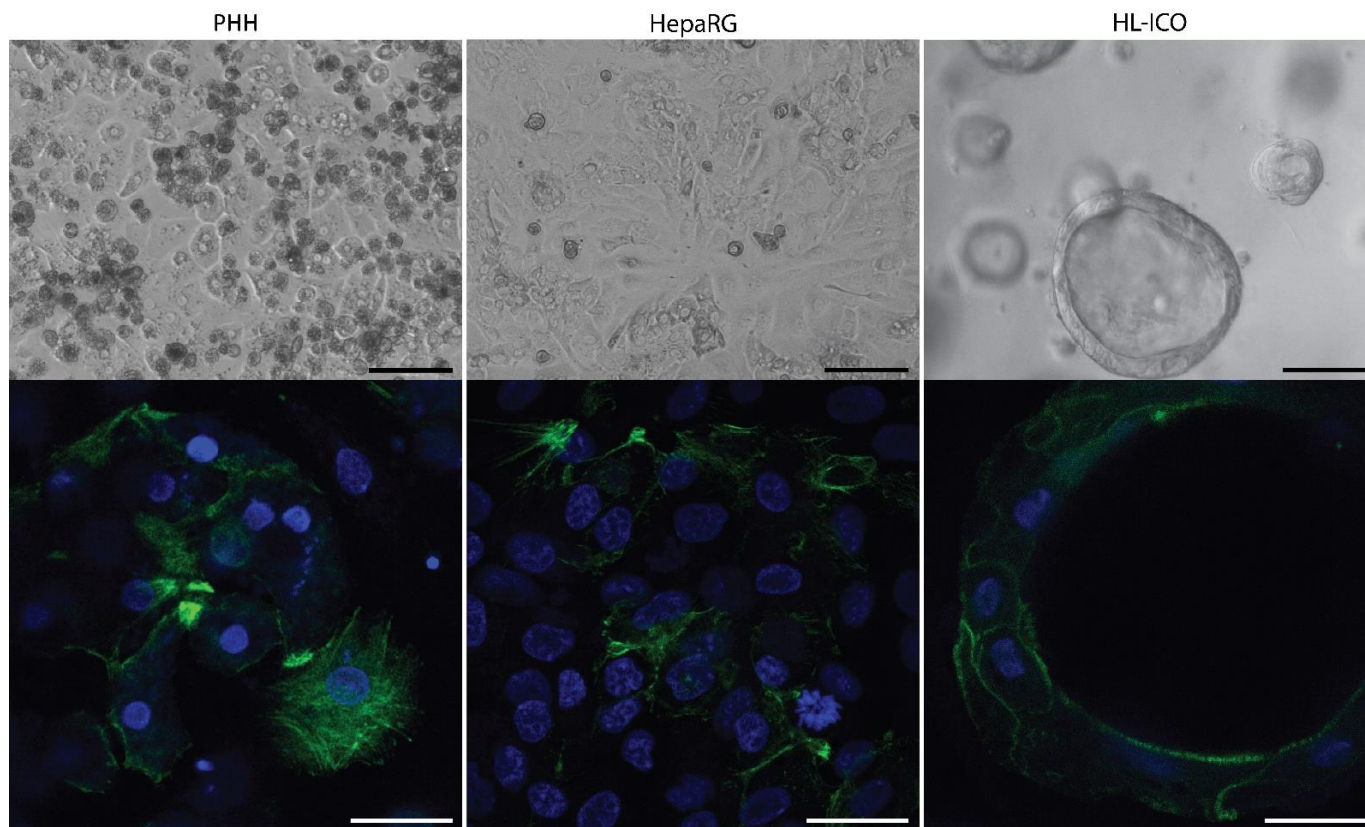


**Figure 1.** Morphology of primary human hepatocytes (PHHs), hepatic cell line HepaRG and hepatocyte-like intrahepatic cholangiocyte organoids (HL-ICOs) on differentiation day 12. Top: Brightfield pictures of morphology. Scale bar = 100  $\mu\text{m}$ . Bottom: Phalloidin staining (green) of filamentous actin. Scale bar = 25  $\mu\text{m}$ .

### 2.1. Expression of Phase I and II Enzymes, and Hepatic Transporters

Gene expression levels of selected key genes involved in phase I and II drug metabolism and hepatic transporters were examined in liver tissue from two donors, primary human hepatocytes, differentiated HepaRG and ICOs (3 donors) in expansion condition (EM), and hepatic differentiation condition (DM day 5 and 12).

Expression levels in ICOs of most phase I enzymes including major cytochrome P450 enzymes, such as CYP1A2, CYP2B6, and CYP2D6, improved upon hepatocyte differentiation but showed low expression compared to PHHs and HepaRGs (Figure 2). Expression of major CYP enzymes CYP3A4 and CYP2C9 increased upon ICO differentiation, where expression levels at day 12 of differentiation were higher compared to HepaRGs. CYP1A1 expression levels also increased upon differentiation of ICOs, where expression levels at day 12 of differentiation were higher compared to PHHs and HepaRGs. Other upregulated genes upon hepatic differentiation compared to expansion condition were (among others) CYP2C19, CES1, FMO4, and FMO5 in phase I, UGT2B7, UGT2B11, SULT1C2 in phase II,

and transporters ABCG2, ABCB1, and ABCB11 (Figure 2). Hepatic transporters ABCB1, ABCB11, and ABCB8 were more highly expressed in HL-ICOs compared to HepaRGs.

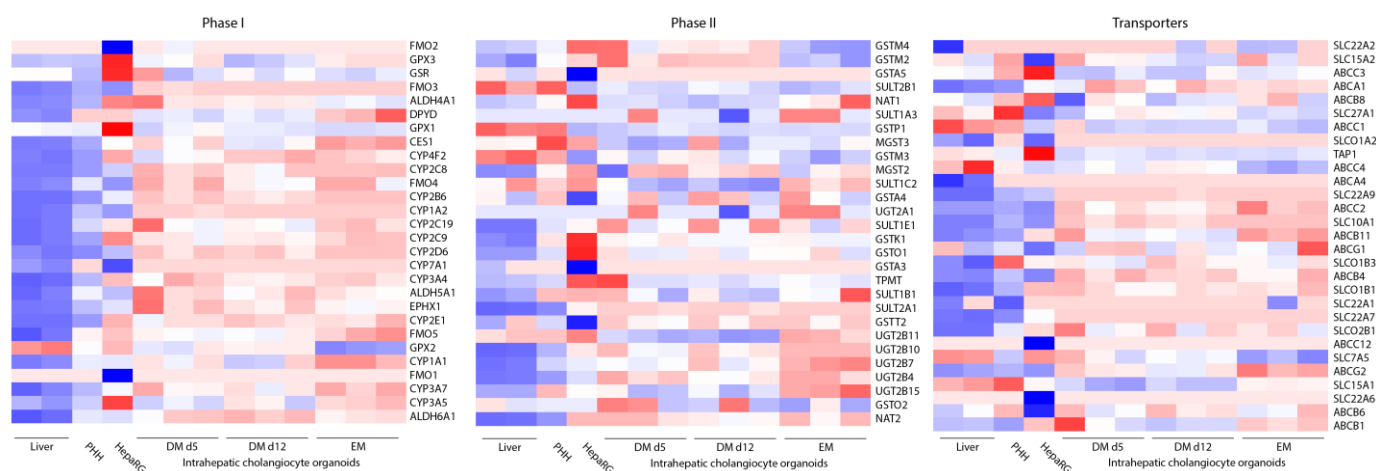


**Figure 2.** Heatmap showing the mRNA expression of intrahepatic cholangiocyte organoids from three independent donors in expansion (EM) and after hepatocyte differentiation (DM day 5 and day 12) compared with that of liver tissue, primary human hepatocytes (PHHs) and HepaRGs involved in drug metabolism (phase I ( $n = 28$ ), phase II ( $n = 28$ ), and transport ( $n = 29$ )). Red indicates low expression. Blue indicates high expression.

Intraindividual differences between the three ICO donors could be observed in (among others) phase I enzymes CYP2C8, CYP2C19, CYP3A5, and CES1, phase II enzymes SULT1B1, UGT2B15, UGT2A1, SULT1A3, and transporters ABCB6, ABCG1, ABCB8, and SLCO2B1.

CYP family members were thoroughly studied to examine their role in DILI, especially the members most abundantly present in humans: CYP3A4, CYP2E1, CYP2C9, CYP2C8, and CYP1A2. Based on the increased expression of these CYP enzymes, differentiation day 12 was selected for further experiments. Due to practical considerations, four different ICO donors were used in further experiments.

## 2.2. Phase I and II Enzyme Activity

The activities of cytochrome P450 enzymes 1A2, 2B6, 2C9, 2D6, 2E1, and 3A4 and UGT were examined in the three hepatic cell models. Cells were exposed to two cocktails of, in total, seven specific enzyme substrates. Metabolite formation was used as a measure for activity of the specific CYP enzyme and UGT (Figure 3). For each cell model, metabolite formation was measured at three timepoints, which differed per hepatic cell model (HL-ICOs: 4, 8, 24 h; PHH: 1, 2, 4 h; HepaRG: 2, 4, 8 h). Metabolite formation rates were calculated using the linear correlation of formed metabolite (pmol/ $10^6$  cells) in time (Table 1).

**Table 1.** Comparison of enzyme-specific metabolite formation rates in HL-ICOs, PHHs and HepaRG.

	HL-ICOs				PHH	HepaRG
CYP1A2	nd	0.01249	0.01293	nd	0.4269	0.03237 (nd–0.08552)
CYP2B6	nd	nd	nd	nd	50.13	1.228 (0.9913–1.358)
CYP2C9	nd	nd	nd	nd	15.33	2.161 (1.365–2.521)
CYP2D6	nd	nd	nd	nd	9.601	0.1656 (0.1567–0.2866)
CYP2E1	nd	nd	nd	nd	nd	nd
CYP3A4	0.3294	0.3603	2.098	0.2278	1.680	0.3136 (0.2645–0.3296)
UGT	13.18	38.93	22.89	8.778	86.79	158.9 (132.6–225.4)

Values presented are the metabolite formation rates (pmol/min/ $10^6$  cells). Hepatocyte-like ICOs (HL-ICOs; differentiation day 12): values are calculated per donor. PHH: Value represents the mean of a technical triplicate. HepaRG: Value represents median of three independent experiments, minimum and maximum formation rate within brackets. nd: not determinable (i.e., no metabolite formation).

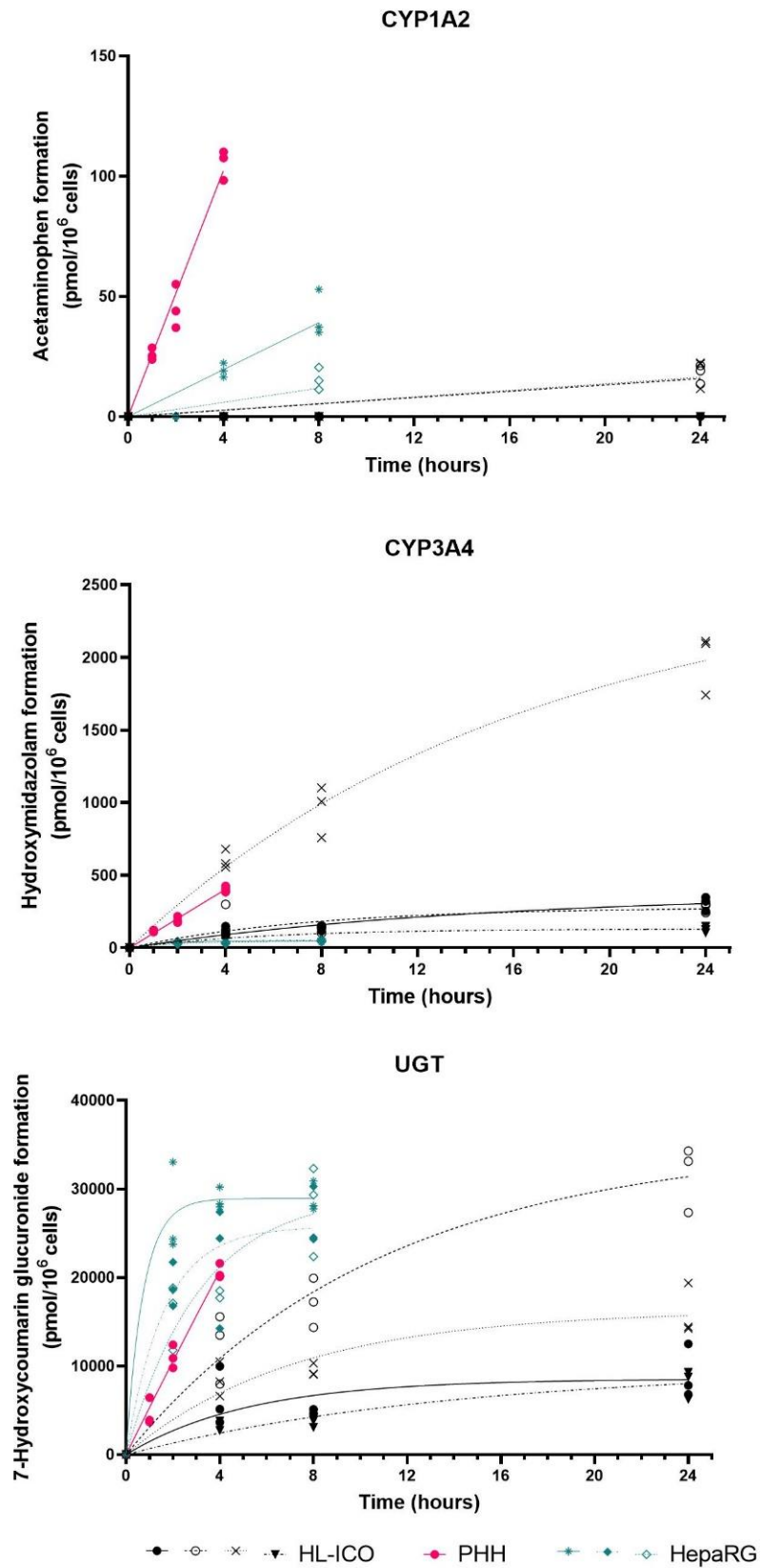


**Figure 3.** Metabolite formation as a measure of enzyme activity in hepatocyte-like intrahepatic cholangiocyte organoids (HL-ICOs) on differentiation day 12, primary human hepatocytes (PHHs), and HepaRG cells. HL-ICO: each black symbol indicates a different donor ( $n = 4$ ). HepaRG: Each green symbol represents an independent experiment. PHH: Technical triplicates are shown in pink.

Activity could not be determined in HL-ICOs for CYP2B6, CYP2C9, CYP2D6, and CYP2E1, as there was no metabolite formation. The chlorzoxazone metabolite (6-hydroxy-chlorzoxazone formed by CYP2E1) was also not formed by PHHs, and in HepaRG cells only in one (out of three) experiments at the last timepoint (8 h) of incubation, indicating low activity for CYP2E1 (data not shown). Metabolite formation by CYP2B6 (hydroxybupropion), CYP2C9 (4-hydroxytolbutamide), and CYP2D6 (dextrorphan) in both HepaRGs and PHHs showed a linear trend (Supplemental Figure S2). In all three systems, depletion of bupropion was observed in control (no cells; data not shown), indicating degradation due to other components in the system, such as binding to the polystyrene culture plate.

CYP1A2 activity in HL-ICOs only showed metabolite (acetaminophen) formation in two of the four donors at the last timepoint (24 h) of incubation (Figure 3). CYP1A2 activity in HepaRGs was not consistent over the three independent experiments, as in one of the three experiments no metabolite was formed. CYP1A2 activity in PHHs was highest compared to the other two hepatic cell models. CYP3A4 activity in HL-ICOs showed intraindividual variation, as one of the four tested donors showed CYP3A4 activity comparable to PHHs (Figure 3; Table 1). CYP3A4 activity in the other three donors was comparable to HepaRGs. Glucuronidation of 7-hydroxycoumarin by UGT showed complete depletion of parent compound 7-hydroxycoumarin in all three hepatic models. In PHHs and HepaRGs, metabolite formation was to the same extent as the parent compound; however, in HL-ICOs, metabolite formation was only 24–72% of the parent compound (data not shown). UGT activity in HL-ICOs was lower compared to PHHs and HepaRGs and was variable between the different ICO donors (Figure 3; Table 1).

### 2.3. Cytotoxicity

HL-ICOs (four independent donors), PHHs, and the hepatic cell line HepaRG (three independent experiments) were exposed to five known hepatotoxic compounds for 48 h (Table 2; Figure 4). Concentration ranges differed per compound but were the same for the different hepatic cell models.

**Table 2.** Determined EC50 values in HL-ICOs, PHH, and HepaRGs.

	HL-ICOs				PHH	HepaRG
Acetaminophen	24,870	24,630	26,840	24,010	4186	4036 (3465–6045)
Diclofenac	>500	>500	>500	475.5	421.2	351.7 (272.4–434.9)
Perhexiline	>31.5	9.675	>31.5	>31.5	8.072	25.97 (10.45–26.37)
Troglitazone	42.80	90.83	23.13	24.40	57.09	45.15 (14.89–45.17)
Valproic Acid	>10,000	>10,000	>10,000	>10,000	9885	4582 (4168–6066)

Values in  $\mu\text{M}$ . HepaRG cells: the median value of three independent experiments is shown with the minimum and maximum EC50 within brackets. HL-ICOs (differentiation day 12): determined EC50 values are shown for each donor separately.

The determined EC50 of acetaminophen for the four ICO donors (24.01–24.87 mM) was higher compared to that for PHHs (4.19 mM) and the hepatic cell line HepaRG (ranging from 3.46 to 6.04 mM). For diclofenac, the EC50 was determined for only one of the tested ICO donors (475.5  $\mu\text{M}$ ), while for the other three ICO donors, the EC50 was higher than the highest tested concentration (500  $\mu\text{M}$ ). The EC50 of diclofenac for PHHs (421.2  $\mu\text{M}$ ) and HepaRGs (ranging from 272.4 to 434.9  $\mu\text{M}$ ) was fairly similar. Perhexiline exposure showed no cytotoxicity in three ICO donors; in one donor, cytotoxicity was observed in the highest concentration (32  $\mu\text{M}$ ; EC50 of 9.675  $\mu\text{M}$ ). PHHs and HepaRGs had a similar cytotoxicity curve (PHH: 8.072  $\mu\text{M}$ ; HepaRG: ranging from 10.45 to 26.37  $\mu\text{M}$ ). The determined EC50 of troglitazone in HL-ICOs and HepaRGs was in the same range and followed a similar trend (HL-ICOs: ranging from 23.13–90.83  $\mu\text{M}$ ; HepaRG: ranging from 14.89 to 45.17  $\mu\text{M}$ ). The EC50 of valproic acid could not be determined in HL-ICOs (PHH: 9.88 mM; HepaRG: ranging from 4.17 to 6.07 mM).

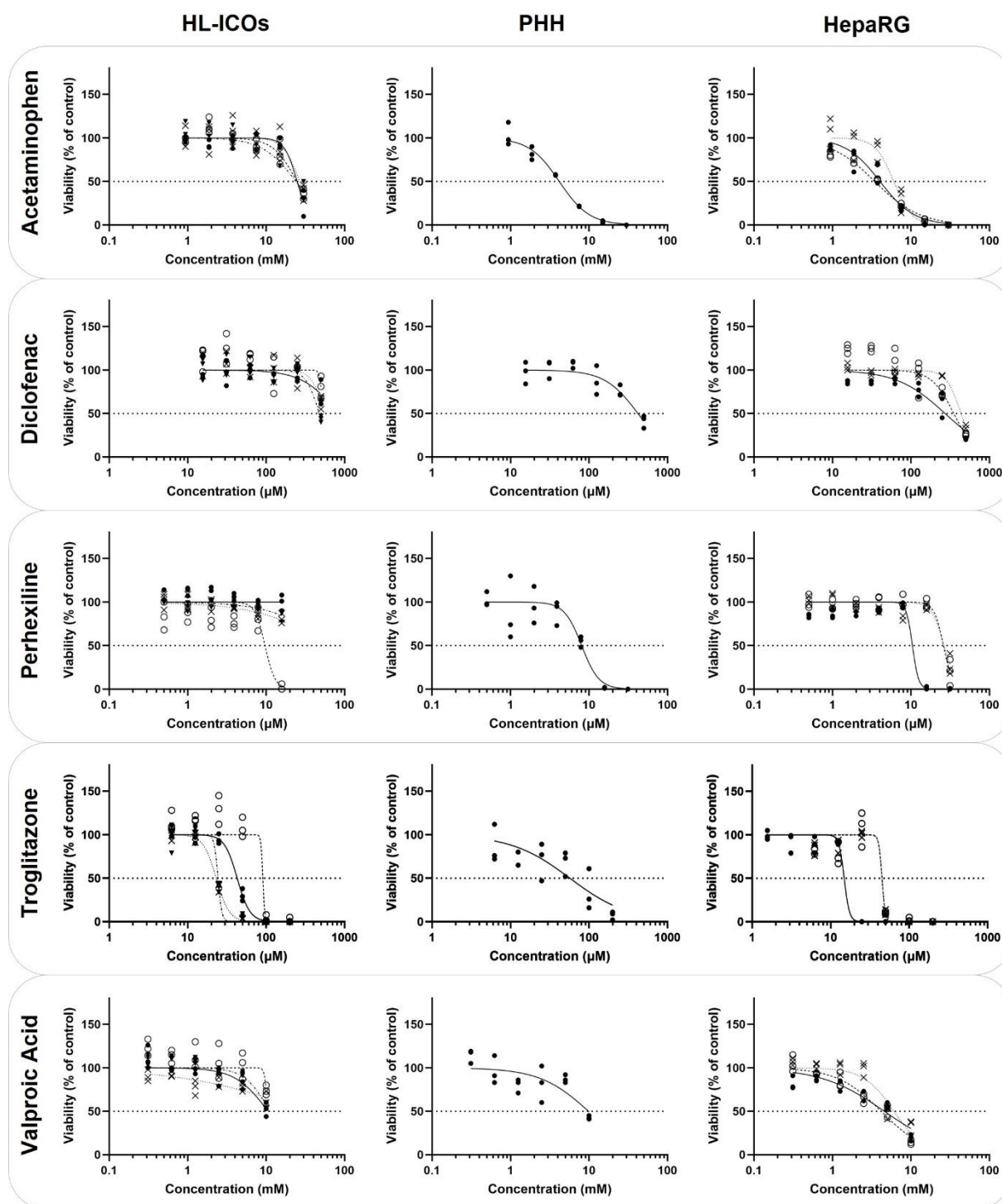


**Figure 4.** Sensitivity to known hepatotoxic compounds of HL-ICOs, PHHs, and HepaRGs. PHHs, HepaRG cells, and HL-ICOs (differentiation day 12) were exposed to acetaminophen, diclofenac, perhexiline, troglitazone, and valproic acid for 48 h (single dose). Data are presented as the percentage relative to the viability of (vehicle-treated) controls. For PHHs, one replicate experiment is shown. For HepaRG cells, three replicate experiments (different symbols) are shown (replicate experiments can be different between tested compounds). For HL-ICOs, four replicate experiments using different donors are shown, represented by different symbols. For all cell models, three replicate measurements per concentration are shown. Dashed line indicates 50% viability.

### 3. Discussion

Emerging advances in the field of *in vitro* and *in silico* toxicity testing attempt to meet the need for reliable human-based safety assessment in drug development [36,37]. Well-established *in vitro* models, such as PHHs or human hepatic cancer cell lines, are used for high-throughput toxicity screens [38–40] and/or in studies of the mechanisms driving DILI [41]. Intrahepatic cholangiocyte organoids (ICOs) have been recently described as a donor-derived hepatic *in vitro* model with potential in disease modelling and regenerative medicine [29]. Here, we explored the potential of liver-derived hepatocyte-like ICOs (HL-ICOs) in *in vitro* toxicity testing by quantifying the expression and activity of genes involved in drug metabolism and exposure to well-known hepatotoxicants.

Drug metabolism is of particular interest due to (de)toxification of compounds in the liver by phase I or phase II enzymes and excretion of compounds by hepatic transporters [6,12]. Two timepoints of hepatic differentiation of ICOs were included in the RNAseq analysis, as hepatic markers are known to rise and fall asynchronously, resulting in no optimal differentiation day for all markers [35]. Based on increased expression levels of CYP enzymes and hepatic transporters on the late differentiation day (d12), further experiments were executed in this differentiation window. In ICOs, the gene expression of abundant CYP enzymes in human CYP2B6, CYP2C9, and CYP2D6 improved upon hepatic differentiation; however, expression was lower than in PHHs. This was reflected in the CYP activity results, even though different ICO donors were used. CYP3A4 expression, which is responsible for metabolism of most therapeutic categories [5], was increased upon differentiation to levels higher than in HepaRG, which was reflected in the CYP activity data. One donor reached a formation rate comparable to PHHs, indicating the interindividual differences in CYP expression [5]. Even though CYP2D6 and CYP2C9 are highly variable in the human population [8], the used ICO donors did not show activity of these enzymes, as metabolite formation was not measurable. Expression of phase II enzymes in ICOs was generally higher than that of phase I enzymes. Notably, we observed relatively high expression of phase II enzymes in HL-ICOs compared to PHHs and HepaRGs, such as UGT2B11, UGT2B15, SULT1C2, and SULT1B1, suggesting differential activity in phase II metabolism pathways, as was observed by 7-hydroxycoumarin metabolite formation [42].

In order to further elucidate the potential of HL-ICOs in *in vitro* toxicity testing, the sensitivity of HL-ICOs to five well-known hepatotoxicants with different mechanisms of action was examined [43]. The three cell models were exposed to acetaminophen, a classic example of intrinsic DILI due to its predictable and dose-dependent toxicity [44]. The formation of its toxic metabolite NAPQI, catalyzed by CYP2E1, CYP3A4, and CYP1A2, is known to cause subsequent glutathione depletion [44,45]. However, we did not see a donor difference regarding the ICO donor with high CYP3A4 activity. The established EC<sub>50</sub> in HL-ICOs was five-fold higher than those in PHHs and HepaRGs (which were comparable to the literature [19]). This difference could possibly be due to different media compositions (high levels of glutathione increase NAPQI conjugation) or increased activity in the alternative glucuronidation and sulfation pathways, as previously mentioned [45–47]. Exposure to the non-steroidal anti-inflammatory drug (NSAID) diclofenac showed that the sensitivity of one ICO donor was comparable to that of HepaRGs and PHHs [19]. Although no metabolite formation was measurable for CYP2C9 activity in HL-ICOs, the diclofenac data suggested that this specific donor did have CYP2C9 activity, as this CYP enzyme is involved in the bioactivation of diclofenac [48]. Perhexiline is a coronary vasodilator that was withdrawn from the market due to hepatotoxicity and neurotoxicity. The exact mechanism of perhexiline toxicity has not yet been clarified; however, it is suggested that perhexiline hepatotoxicity is mostly caused by the parent drug and that CYP2D6 is involved in the detoxification [49,50]. The observed cytotoxicity for PHHs and HepaRGs and one ICO donor was comparable to the literature [49]. Notably, no cytotoxicity was observed in three ICO donors, while higher toxicity was expected in a system with low metabolism [50,51]. Troglitazone, a thiazolidinedione derivative, is known to cause parent compound toxicity, but its metabolites also cause toxicity, such as inhibition of hepatic transporter BSEP,



resulting in intrahepatic cholestasis [52]. Established EC50s by troglitazone exposure were comparable to those reported in the literature [19], even though a different trend was observed for PHHs compared to HepaRGs and HL-ICOs. Slight interindividual differences in cytotoxicity were observed between the ICO donors; however, this could not be linked to CYP and UGT activity data in this study. In the literature, troglitazone cytotoxicity cannot be correlated to CYP activity either; however, sulfotransferases possibly play a role in its cytotoxicity [53,54]. Anticonvulsant valproic acid hepatotoxicity is mainly caused by its metabolites, resulting in drug-induced steatosis [55]. Toxic metabolite formation is catalyzed by CYP2C9 and CYP2B6, the activity of which could not be measured in HL-ICOs. For HL-ICOs, an EC50 could not be established; however, the trend seems comparable to that of PHHs.

To improve the comparison between different cell systems, it is essential to determine the concentration that is actually available to be taken up by the cells in the *in vitro* system. In the case of lipophilic compounds such as perhexiline, *in vitro* system components such as Matrigel or medium components can decrease this available concentration [56,57]. In the case of bupropion (CYP2B6 activity), abiotic degradation of the compound was observed, especially in the HL-ICOs. Determining the real *in vitro* dose facilitates reliable extrapolation of *in vitro* data towards *in silico* models [18,58].

The current state of drug metabolism in HL-ICOs showed comparable levels for, among others, CYP3A4. However, the expression and activity of other enzymes, such as CYP2B6 and CYP2D6, need improvement in HL-ICOs compared to PHHs and HepaRGs. The donor-derived origin of the HL-ICOs was clearly represented in the CYP3A4, CYP1A2, and UGT activity data and in gene expression levels, such as for CYP2C8, CES1, and SLCO2B1, which are known to have polymorphisms [8,59,60]. Genotyping ICOs of different donors would give more insight into the donor differences and enable the selection of a panel of donors with slow/fast metabolizers or specific polymorphisms associated with DILI [48]. Moreover, extending the set of donors could also provide insight into sex-specific drug responses [61]. A more mechanistic approach would help in further characterization of HL-ICOs as an *in vitro* toxicity model [41,62]. Recent papers explored the potential of HL-ICOs with a more mechanistic approach to study the applicability of HL-ICOs as an *in vitro* model for cholestasis [63] and phospholipidosis [31]. While bile production in ICOs was shown to be low compared to HepaRGs and PHHs, ICOs were more sensitive in drug-induced phospholipidosis screening compared to HepG2 cells. A unique feature of HL-ICOs is their polarization and relative expression of hepatic transporters compared to PHHs, suggesting possibilities for HL-ICOs in toxicity screens involving transporters that are important in toxicity prediction [64]. Further characterization of the functionality of HL-ICOs, for example, using a comprehensive phase II enzyme activity assay [65,66], and their predictive potential to compound toxicity using a more extensive set of test compounds and readouts in a high-throughput fashion [67,68], will illustrate their potential in *in vitro* toxicity testing.

## 4. Materials and Methods

### 4.1. Cell Culture

LiverPool cryoplateable hepatocytes (pool of 10 donors, mixed gender; BioIVT, Hicksville, NY, USA) were cultured in a collagen I (Sigma-Aldrich, St Louis, MO, USA) sandwich in INVITROGRO CP medium (BioIVT) complemented with the TORPEDO Antibiotic mix (BioIVT). Seeding density was 49,000 cells/well in a 96-well plate (cytotoxicity assay) or 350,000 cells/well in a 24-well plate (CYP activity assay), according to the manufacturer's instructions. Exposure of the hepatocytes was started 48 h after seeding. For exposure assays, INVITROGRO HI medium (BioIVT) was used, as recommended.

Undifferentiated HepaRG cells were purchased from Biopredic International (Saint Grégoire, France). Cells were cultured (passage number between p18 and p28) in T75 flasks in culture medium consisting of William's E medium (without phenol red; Thermo Fisher Scientific, Waltham, MA, USA) supplemented with 1% (*v/v*) penicillin-streptomycin

(Thermo Fisher Scientific), 10% (*v/v*) fetal bovine serum (FBS; Thermo Fisher Scientific), 50  $\mu$ M hydrocortisone 21-hemisuccinate (Sigma-Aldrich, St Louis, MO, USA), 2 mM GlutaMax (Thermo Fisher Scientific) and 5  $\mu$ g/mL insulin (Sigma-Aldrich). For differentiation, cells were cultured for 7–10 days and upon confluence, the monolayer was switched to differentiation medium (culture medium supplemented with 1% (*v/v*) DMSO). After differentiation, cells were trypsinized using TrypLE (Thermo Fisher Scientific) and seeded at a density of 65,000 cells/well in a 96-well plate (cytotoxicity assay) or 130,000 cells/well in a 24-well plate (CYP activity assay). Cells were allowed to attach for 24 to 48 h. Before exposure, cells were washed with assay medium (culture medium without FBS), after which exposure was started.

Intrahepatic cholangiocyte organoids (ICOs) were isolated from healthy liver biopsies that were obtained during liver transplantation at the Erasmus Medical Center Rotterdam in accordance with the ethical standards of the institutional committee to use the tissue for research purposes (ethical approval number MEC 2014-060). The procedure was in accordance with the Helsinki Declaration of 1975, and informed consent in writing was obtained from each patient. Obtained human liver material was frozen down in Recovery Cell Freezing Medium for future experiments or used for organoid isolation directly. Organoid isolation is described by Schneeberger et al. 2018 [35]. In short, small pieces of tissue were enzymatically digested at 37 °C. The supernatant was collected every hour, and fresh enzyme-supplemented medium was added to the remaining tissue until only ducts and single cells were visible. Cells were washed with DMEM GlutaMax (supplemented with 1% (*v/v*) FBS and 1% (*v/v*) P/S) and spun down at 453 g for 5 min.

The cell suspension was cultured in Matrigel™ (Corning, New York, NY, USA) droplets in expansion medium (EM) until organoids were formed, as previously described [28]. EM consisted of Advanced DMEM/F12 (Life Technologies) supplemented with 1% (*v/v*) penicillin-streptomycin (Life Technologies), 1% (*v/v*) GlutaMax (Life Technologies), 10 mM HEPES (4-(2-hydroxyethyl)-1-piperazineethanesulfonic acid, Life Technologies), 2% (*v/v*) B27 supplement without vitamin A (Invitrogen, Carlsbad, CA, USA), 1% (*v/v*) N2 supplement (Invitrogen), 10 mM nicotinamide (Sigma-Aldrich, St Louis, MO, USA), 1.25 mM N-acetylcysteine (Sigma-Aldrich), 10% (*v/v*) R-spondin-1 conditioned medium (the Rspo1-Fc-expressing cell line was a kind gift from Calvin J. Kuo), 10  $\mu$ M forskolin (Sigma-Aldrich), 5  $\mu$ M A83-01 (transforming growth factor beta inhibitor; Tocris Bioscience, Bristol, UK), 50 ng/mL EGF (Invitrogen), 25 ng/mL HGF (Peprotech, Rocky Hill, NJ, USA), 0.1  $\mu$ g/mL FGF10 (Peprotech) and 10 nM recombinant human (Leu15)-gastrin I (Sigma-Aldrich). Medium was changed twice a week. Passaging occurred every 7–10 days at ratios ranging between 1:2 and 1:4. All cultures were kept in a humidified atmosphere of 95% air and 5% CO<sub>2</sub> at 37 °C. Organoids were primed for differentiation with BMP7 (25 ng/mL, Peprotech) through spiking EM 3 days before shifting to hepatic differentiation medium (DM). DM consisted of EM without R-spondin-1, FGF10, and nicotinamide, supplemented with 100 ng/mL FGF19 (Peprotech), 500 nM A83-01 (Tocris Bioscience), 10  $\mu$ M DAPT (Selleckchem, Munich, Germany), 25 ng/mL BMP-7 (Peprotech), and 30  $\mu$ M dexamethasone (Sigma-Aldrich). Organoids were kept on DM for up to 12 days. For exposure experiments, differentiation assay medium was prepared to reduce antioxidants in the medium. This assay medium consisted of DMEM GlutaMAX instead of DMEM-F12 medium complemented with the same components as differentiation medium excluding GlutaMAX, B27, and NAC. In 96-well format (cytotoxicity assay), 12,000 cells in 9  $\mu$ L Matrigel per well were plated at the start of differentiation, and exposure was started at day 10 of differentiation for 48 h. In 24-well format (CYP activity assay), cells were densely plated in a fresh Matrigel droplet (50  $\mu$ L) upon the start of differentiation, and cells were exposed to the CYP substrate cocktail on day 12 of differentiation. The median cell count after CYP cocktail assay was 290,415 (46,968–812,410).

All cell cultures were performed in a humidified atmosphere with 5% CO<sub>2</sub> at 37 °C. The cellular morphology of the three cell models was visualized by immunofluorescence staining with a filamentous actin (F-actin) probe conjugated to a photostable green-

fluorescent Alexa Fluor 488 dye (ThermoFisher) using confocal laser scanning microscopy (SP8, Leica Microsystems, the Netherlands), as described by Wang et al., 2022 [69].

#### 4.2. Whole Genome RNA Sequencing

For mRNA sequencing, ICOs of three independent donors in expanding conditions and differentiated for 5 and 12 days were collected. Additionally, freshly isolated hepatocytes and liver tissue were used. RNA was isolated using the RNeasy Mini Kit (Qiagen, Hilden, Germany) according to the manufacturer's instructions. As described in Schneeberger et al. (2018), Poly(A) Beads (NEXTflex, Bio Scientific, Austin, TX) were used to isolate the polyadenylated mRNA fraction. Sequencing libraries were prepared using the Rapid Directional RNA-Seq Kit (NEXTflex). Illumina NextSeq500 sequencing produced single-end 75-base-pair long reads. RNA-sequencing reads were mapped using STAR (v2.4.2a). Read groups were added to the BAM files with Picard's AddOrReplaceReadGroups (v1.98) and sorted with Sambamba (v0.4.5). Transcript abundances were quantified with HTSeq-count (v0.6.1p1) using the union mode. The raw files were uploaded to Gene Expression Omnibus (GEO) database (accession number GSE123498). RNA sequencing data of the HepaRG cell line were retrieved from the GEO database (accession number GSE14654). Genes important in drug metabolism were selected [70]. Heatmaps were generated using edgeR.

#### 4.3. Cytochrome P450 Activity

CYP activity was assessed by the addition of a CYP substrate cocktail prepared in assay medium (see methods cell culture). Two CYP cocktail sets were prepared to expose the hepatic cell models (Table 3): set A included phenacetin (CYP1A2, 15  $\mu$ M), midazolam (CYP3A4, 5  $\mu$ M), dextromethorphan (CYP2D6, 15  $\mu$ M), tolbutamide (CYP2C9, 20  $\mu$ M); and set B included 7-hydroxycoumarin (UGT, 12  $\mu$ M), chlorzoxazone (CYP2E1, 25  $\mu$ M) and bupropion (CYP2B6, 20  $\mu$ M) [71,72]. At three cell model-specific timepoints (PHHs: 1, 2, 4 h; HepaRGs: 2, 4, 8 h; ICOs: 4, 8, 24 h), 400  $\mu$ L exposure medium was placed into glass vials containing 400  $\mu$ L acidified MeOH (0.1% (*v/v*) formic acid). The samples were stored at  $-20^{\circ}\text{C}$  until analysis. Prior to LC-MS/MS analysis, samples were centrifuged for 10 min at 1250 g to precipitate any protein.

**Table 3.** Information on enzyme activity cocktails.

	Enzyme	Parent Compound	CAS Number	Dosed Concentration ( $\mu$ M)
Cocktail A	CYP1A2	Phenacetin	62-44-2	15
		Acetaminophen	103-90-2	
	CYP3A4	Midazolam	59467-70-8	5
		Midazolam-OH	59468-90-5	
	CYP2D6	Dextromethorphan	125-71-3	15
		Dextrorphan	143-98-6	
CYP2C9	Tolbutamide	64-77-7	20	
	4OH-Tolbutamide	5719-85-7		
Cocktail B	UGT	7-OH Coumarin	93-35-6	12
		7-OH Coumarin Glucuronide	66695-14-5	
	CYP2E1	Chlorzoxazone	95-25-0	25
		6OH-Chlorzoxazone	1750-45-4	
CYP2B6	Bupropion	31677-93-7	20	
	OH-Bupropion	92264-81-8		

Standards for LC-MS/MS analysis of phenacetin, acetaminophen, midazolam, hydroxy-midazolam, dextromethorphan, dextropropion, tolbutamide, 4-hydroxy-tolbutamide, 7-hydroxy-coumarin, 7-hydroxy-coumarin glucuronide, chlorzoxazone, 6-hydroxy-chlorzoxazone, bupropion, and hydroxy-bupropion were prepared in the same matrix as the medium extracts. All chemicals were obtained from Sigma-Aldrich. All previously listed substrates and metabolites were analyzed in a single run using a Shimadzu triple-quadrupole LCMS 8050 system with two Nexera XR LC-20AD pumps, a Nexera XR SIL-20AC autosampler, a CTO-20AC column oven, an FCV-20AH2 valve unit (Shimadzu, 's Hertogenbosch, the Netherlands). The substrates and metabolites were separated on a Synergi Polar-RP column (150 × 2.0 mm, 4 μm, 80 Å) with a 4 × 2 mm C18 guard column (4 × 2 mm; Phenomenex, Torrance, CA, USA). The mobile phase consisted of 0.1% (*v/v*) formic acid in Millipore (A) and 0.1% (*v/v*) formic acid in MeOH (pH 2.7; B), and was set as 100% A (0–1 min), 100% to 5% A (1–8 min), 5% A (8–9 min), 5% to 100% A (9–9.5 min), and 100% A (9.5–12.5 min). The total run time was 12.5 min, and the flow rate was 0.2 mL/min. Peaks were integrated using LabSolutions software.

#### 4.4. Cytotoxicity

Cells plated in 96-well plates were exposed to a concentration range (six concentrations in 2x dilution) of five known hepatotoxic compounds for 48 h (single dose). Acetaminophen (CAS 103-90-2; 30 mM) and valproic acid (CAS 1069-66-5; 10 mM) were directly dissolved in assay medium (previously described for each hepatic cell model). Diclofenac (CAS 15307-79-6; 100 mM), perhexiline (CAS 6724-53-4; 6.3 mM), and troglitazone (CAS 15307-79-6; TRC, Toronto, Canada; 40 mM) were dissolved in dimethyl sulfoxide (DMSO), which was 200x diluted in the highest exposure concentration. For the latter, vehicle control (0.5% (*v/v*) DMSO) was used in the exposure experiments. All chemicals were obtained from Sigma-Aldrich, unless stated otherwise. Dose ranges of exposure: acetaminophen 0.94–30 mM; diclofenac 15.57–500 μM; perhexiline 0.5–31.5 μM; troglitazone 6.25–200 μM; valproic acid 0.31–10 mM.

#### 4.5. Cell Viability

The viability of exposed cells was determined by cellular ATP levels using the CellTiter-Glo Luminescent Cell Viability Assay (Promega, Madison, WI, USA). The CellTiter Glo reagent was prepared according to the manufacturer's instructions. Briefly, the culture plate was equilibrated at room temperature for 30 min. Medium was removed from the plate, after which phosphate-buffered saline (PBS) and the CellTiter Glo reagent were added to each well in equal volumes. The plate was mixed for 2 min on an orbital shaker and incubated for an additional 10 min at room temperature. Luminescence was measured on the TriStar2 (Berthold Technologies, Bad Wildbad, Germany), and samples were normalized to (vehicle) control.

## 5. Conclusions

Here, we explored the levels of drug metabolism in hepatocyte-like intrahepatic cholangiocyte organoids and their potential in *in vitro* toxicity testing. We found that although the hepatic differentiation and the expression and activity of most drug metabolizing enzymes in ICOs were still below that of PHHs and HepaRGs, HL-ICOs could be a valuable platform for individualized toxicity screenings in the future. Further elucidation of enzyme and transporter activity in drug metabolism in HL-ICOs is needed to better define their potential. Additionally, exposure to a more extensive compound set including subtoxic concentrations and mechanistic studies would give more insight into the specific application of HL-ICOs in *in vitro* toxicity testing.

**Supplementary Materials:** The following supporting information can be downloaded at: <https://www.mdpi.com/article/10.3390/molecules28020621/s1>, Figure S1: Gene expression of hepatic markers upon hepatic differentiation of ICOs; Figure S2: Metabolite formation of bupropion (CYP2B6), tolbutamide (CYP2C9), and dextromethorphan (CYP2D6) in primary human hepatocytes and HepaRGs.

**Author Contributions:** Conceptualization, M.C.B., B.S., K.S. and N.I.K.; methodology, M.C.B., S.P., T.S., Y.T. and S.M.N.; formal analysis, F.G.v.S.; investigation, M.C.B., Y.T., R.-A.S., T.S. and S.M.N.; resources, L.J.W.v.d.L.; writing—original draft preparation, M.C.B.; writing—review and editing, B.S., N.I.K., Y.T., S.P., F.G.v.S., T.S., L.J.W.v.d.L., J.L. and K.S.; visualization, M.C.B., Y.T. and F.G.v.S.; supervision, B.S. and N.I.K.; funding acquisition, B.S. and N.I.K. All authors have read and agreed to the published version of the manuscript.

**Funding:** This work is part of the research program Applied and Engineering Sciences with project number 15498, which is financed by the Dutch Research Council (NWO).

**Institutional Review Board Statement:** The study was conducted in accordance with the Declaration of Helsinki, and approved by the Institutional Review Board (or Ethics Committee) of Erasmus Medical Center Rotterdam (protocol code MEC 2014-060).

**Informed Consent Statement:** Informed consent was obtained from all subjects involved in the study.

**Data Availability Statement:** Not applicable, except for RNAseq data: GEO accession number GSE14654.

**Conflicts of Interest:** The authors declare no conflict of interest.

## References

1. Issa, N.T.; Wathieu, H.; Ojo, A.; Byers, S.W.; Dakshanamurthy, S. Drug Metabolism in Preclinical Drug Development: A Survey of the Discovery Process, Toxicology, and Computational Tools. *Curr. Drug Metab.* **2017**, *18*, 556–565. [[CrossRef](#)] [[PubMed](#)]
2. Sun, D.; Gao, W.; Hu, H.; Zhou, S. Why 90% of clinical drug development fails and how to improve it? *Acta Pharm. Sin. B* **2022**, *12*, 3049–3062. [[CrossRef](#)]
3. García-Cortés, M.; Ortega-Alonso, A.; Lucena, M.I.; Andrade, R.J. Spanish Group for the Study of Drug-Induced Liver Disease (Grupo de Estudio para las Hepatopatías Asociadas a Medicamentos GEHAM) I Drug-induced liver injury: A safety review. *Expert Opin. Drug Saf.* **2018**, *17*, 795–804. [[CrossRef](#)] [[PubMed](#)]
4. Craveiro, N.S.; Lopes, B.S.; Tomás, L.; Almeida, S.F. Drug Withdrawal Due to Safety: A Review of the Data Supporting Withdrawal Decision. *Curr. Drug Saf.* **2020**, *15*, 4–12. [[CrossRef](#)] [[PubMed](#)]
5. Zanger, U.M.; Schwab, M. Cytochrome P450 enzymes in drug metabolism: Regulation of gene expression, enzyme activities, and impact of genetic variation. *Pharmacol. Ther.* **2013**, *138*, 103–141. [[CrossRef](#)]
6. Utkarsh, D.; Loretz, C.; Li, A.P. In vitro evaluation of hepatotoxic drugs in human hepatocytes from multiple donors: Identification of P450 activity as a potential risk factor for drug-induced liver injuries. *Chem. Biol. Interact.* **2016**, *255*, 12–22. [[CrossRef](#)]
7. Wang, C.W.; Preclaro, I.A.C.; Lin, W.H.; Chung, W.H. An Updated Review of Genetic Associations With Severe Adverse Drug Reactions: Translation and Implementation of Pharmacogenomic Testing in Clinical Practice. *Front. Pharmacol.* **2022**, *13*, 886377. [[CrossRef](#)]
8. Zhou, S.F.; Liu, J.P.; Chowbay, B. Polymorphism of human cytochrome P450 enzymes and its clinical impact. *Drug Metab. Rev.* **2009**, *41*, 89–295. [[CrossRef](#)]
9. Gan, J.; Ma, S.; Zhang, D. Non-cytochrome P450-mediated bioactivation and its toxicological relevance. *Drug Metab. Rev.* **2016**, *48*, 473–501. [[CrossRef](#)]
10. Liu, H.; Sahi, J. Role of Hepatic Drug Transporters in Drug Development. *J. Clin. Pharmacol.* **2016**, *56* (Suppl. 7), S11–S22. [[CrossRef](#)]
11. Jetter, A.; Kullak-Ublick, G.A. Drugs and hepatic transporters: A review. *Pharmacol. Res.* **2020**, *154*, 104234. [[CrossRef](#)] [[PubMed](#)]
12. Gu, R.; Liang, A.; Liao, G.; To, I.; Shehu, A.; Ma, X. Roles of Cofactors in Drug-Induced Liver Injury: Drug Metabolism and Beyond. *Drug Metab. Dispos.* **2022**, *50*, 646–654. [[CrossRef](#)] [[PubMed](#)]
13. Turpeinen, M.; Ghiciuc, C.; Opritou, M.; Tursas, L.; Pelkonen, O.; Pasanen, M. Predictive value of animal models for human cytochrome P450 (CYP)-mediated metabolism: A comparative study in vitro. *Xenobiotica* **2007**, *37*, 1367–1377. [[CrossRef](#)]
14. Hammer, H.; Schmidt, F.; Marx-Stoelting, P.; Pötz, O.; Braeuning, A. Cross-species analysis of hepatic cytochrome P450 and transport protein expression. *Arch. Toxicol.* **2021**, *95*, 117–133. [[CrossRef](#)]
15. Van Norman, G.A. Limitations of Animal Studies for Predicting Toxicity in Clinical Trials: Is it Time to Rethink Our Current Approach? *JACC Basic Transl. Sci.* **2019**, *4*, 845–854. [[CrossRef](#)] [[PubMed](#)]

16. Krewski, D.; Acosta, D.; Andersen, M.; Anderson, H.; Bailar, J.C.; Boekelheide, K.; Brent, R.; Charnley, G.; Cheung, V.G.; Green, S.; et al. Toxicity testing in the 21st century: A vision and a strategy. *J. Toxicol. Environ. Health Part B* **2010**, *13*, 51–138. [[CrossRef](#)] [[PubMed](#)]
17. Zink, D.; Chuah, J.K.C.; Ying, J.Y. Assessing Toxicity with Human Cell-Based In Vitro Methods. *Trends Mol. Med.* **2020**, *26*, 570–582. [[CrossRef](#)]
18. Yadav, J.; El Hassani, M.; Sodhi, J.; Lauschke, V.M.; Hartman, J.H.; Russell, L.E. Recent developments in in vitro and in vivo models for improved translation of preclinical pharmacokinetics and pharmacodynamics data. *Drug Metab. Rev.* **2021**, *53*, 207–233. [[CrossRef](#)]
19. Serras, A.S.; Rodrigues, J.S.; Cipriano, M.; Rodrigues, A.V.; Oliveira, N.G.; Miranda, J.P. A Critical Perspective on 3D Liver Models for Drug Metabolism and Toxicology Studies. *Front. Cell Dev. Biol.* **2021**, *9*, 626805. [[CrossRef](#)]
20. Xu, Q. Human Three-Dimensional Hepatic Models: Cell Type Variety and Corresponding Applications. *Front. Bioeng. Biotechnol.* **2021**, *9*, 730008. [[CrossRef](#)]
21. Zhang, X.; Jiang, T.; Chen, D.; Wang, Q.; Zhang, L.W. Three-dimensional liver models: State of the art and their application for hepatotoxicity evaluation. *Crit. Rev. Toxicol.* **2020**, *50*, 279–309. [[CrossRef](#)] [[PubMed](#)]
22. Kammerer, S. Three-Dimensional Liver Culture Systems to Maintain Primary Hepatic Properties for Toxicological Analysis In Vitro. *Int. J. Mol. Sci.* **2021**, *22*, 10214. [[CrossRef](#)] [[PubMed](#)]
23. Bell, C.C.; Hendriks, D.F.; Moro, S.M.; Ellis, E.; Walsh, J.; Renblom, A.; Fredriksson Puigvert, L.; Dankers, A.C.; Jacobs, F.; Snoeys, J.; et al. Characterization of primary human hepatocyte spheroids as a model system for drug-induced liver injury, liver function and disease. *Sci. Rep.* **2016**, *6*, 25187. [[CrossRef](#)]
24. Zhang, K.; Zhang, L.; Liu, W.; Ma, X.; Cen, J.; Sun, Z.; Wang, C.; Feng, S.; Zhang, Z.; Yue, L.; et al. In Vitro Expansion of Primary Human Hepatocytes with Efficient Liver Repopulation Capacity. *Cell Stem Cell* **2018**, *23*, 806–819. [[CrossRef](#)] [[PubMed](#)]
25. Elaut, G.; Henkens, T.; Papeleu, P.; Snykers, S.; Vinken, M.; Vanhaecke, T.; Rogiers, V. Molecular mechanisms underlying the dedifferentiation process of isolated hepatocytes and their cultures. *Curr. Drug Metab.* **2006**, *7*, 629–660. [[CrossRef](#)]
26. Kim, Y.; Lasher, C.D.; Milford, L.M.; Murali, T.M.; Rajagopalan, P. A comparative study of genome-wide transcriptional profiles of primary hepatocytes in collagen sandwich and monolayer cultures. *Tissue Eng. Part C Methods* **2010**, *16*, 1449–1460. [[CrossRef](#)]
27. Akbari, S.; Arslan, N.; Senturk, S.; Erdal, E. Next-Generation Liver Medicine Using Organoid Models. *Front. Cell Dev. Biol.* **2019**, *7*, 345. [[CrossRef](#)]
28. Huch, M.; Gehart, H.; van Boxtel, R.; Hamer, K.; Blokzijl, F.; Verstegen, M.M.; Ellis, E.; van Wenum, M.; Fuchs, S.A.; de Ligt, J.; et al. Long-term culture of genome-stable bipotent stem cells from adult human liver. *Cell* **2015**, *160*, 299–312. [[CrossRef](#)]
29. Prior, N.; Inacio, P.; Huch, M. Liver organoids: From basic research to therapeutic applications. *Gut* **2019**, *68*, 2228–2237. [[CrossRef](#)]
30. Nuciforo, S.; Heim, M.H. Organoids to model liver disease. *JHEP Rep.* **2020**, *3*, 100198. [[CrossRef](#)]
31. Lee, J.; Han, H.; Lee, S.; Cho, E.; Lee, H.; Seok, J.; Lim, H.S.; Son, W. Use of 3D Human Liver Organoids to Predict Drug-Induced Phospholipidosis. *Int. J. Mol. Sci.* **2020**, *21*, 2982. [[CrossRef](#)] [[PubMed](#)]
32. He, C.; Lu, D.; Lin, Z.; Chen, H.; Li, H.; Yang, X.; Yang, M.; Wang, K.; Wei, X.; Zheng, S.; et al. Liver Organoids, Novel and Promising Modalities for Exploring and Repairing Liver Injury. *Stem Cell Rev. Rep.* **2022**. [[CrossRef](#)]
33. Wang, L.; Li, M.; Yu, B.; Shi, S.; Liu, J.; Zhang, R.; Ayada, I.; Verstegen, M.M.A.; van der Laan, L.J.W.; Peppelenbosch, M.P.; et al. Recapitulating lipid accumulation and related metabolic dysregulation in human liver-derived organoids. *J. Mol. Med.* **2022**, *100*, 471–484. [[CrossRef](#)] [[PubMed](#)]
34. Shiota, J.; Samuelson, L.C.; Razumilava, N. Hepatobiliary Organoids and Their Applications for Studies of Liver Health and Disease: Are We There Yet? *Hepatology* **2021**, *74*, 2251–2263. [[CrossRef](#)] [[PubMed](#)]
35. Schneeberger, K.; Sánchez-Romero, N.; Ye, S.; van Steenbeek, F.G.; Oosterhoff, L.A.; Pla Palacin, I.; Chen, C.; van Wolferen, M.E.; van Tienderen, G.; Lieshout, R.; et al. Large-Scale Production of LGR5-Positive Bipotential Human Liver Stem Cells. *Hepatology* **2020**, *72*, 257–270. [[CrossRef](#)] [[PubMed](#)]
36. Vinken, M.; Benfenati, E.; Busquet, F.; Castell, J.; Clevert, D.A.; de Kok, T.M.; Dirven, H.; Fritsche, E.; Geris, L.; Gozalbes, R.; et al. Safer chemicals using less animals: Kick-off of the European ONTOX project. *Toxicology* **2021**, *458*, 152846. [[CrossRef](#)]
37. Chang, X.; Tan, Y.M.; Allen, D.G.; Bell, S.; Brown, P.C.; Browning, L.; Ceger, P.; Gearhart, J.; Hakkinen, P.J.; Kabadi, S.V.; et al. IVIVE: Facilitating the Use of In Vitro Toxicity Data in Risk Assessment and Decision Making. *Toxics* **2022**, *10*, 232. [[CrossRef](#)]
38. Schadt, S.; Simon, S.; Kustermann, S.; Boess, F.; McGinnis, C.; Brink, A.; Lieven, R.; Fowler, S.; Youdim, K.; Ullah, M.; et al. Minimizing DILI risk in drug discovery—A screening tool for drug candidates. *Toxicol. In Vitro* **2015**, *30*, 429–437. [[CrossRef](#)]
39. Tolosa, L.; Gómez-Lechón, M.J.; Jiménez, N.; Hervás, D.; Jover, R.; Donato, M.T. Advantageous use of HepaRG cells for the screening and mechanistic study of drug-induced steatosis. *Toxicol. Appl. Pharmacol.* **2016**, *302*, 1–9. [[CrossRef](#)]
40. Vorrink, S.U.; Zhou, Y.; Ingelman-Sundberg, M.; Lauschke, V.M. Prediction of Drug-Induced Hepatotoxicity Using Long-Term Stable Primary Hepatic 3D Spheroid Cultures in Chemically Defined Conditions. *Toxicol. Sci.* **2018**, *163*, 655–665. [[CrossRef](#)]
41. Arnesdotter, E.; Gijbels, E.; Dos Santos Rodrigues, B.; Vilas-Boas, V.; Vinken, M. Adverse Outcome Pathways as Versatile Tools in Liver Toxicity Testing. *Methods Mol. Biol.* **2022**, *2425*, 521–535. [[CrossRef](#)] [[PubMed](#)]
42. Feng, W.Y.; Wen, J.; Stauber, K. In vitro Drug Metabolism Investigation of 7-Ethoxycoumarin in Human, Monkey, Dog and Rat Hepatocytes by High Resolution LC-MS/MS. *Drug Metab. Lett.* **2018**, *12*, 33–53. [[CrossRef](#)]

43. Dragovic, S.; Vermeulen, N.P.E.; Gerets, H.H.; Hewitt, P.G.; Ingelman-Sundberg, M.; Park, B.K.; Juhila, S.; Snoeys, J.; Weaver, R.J. Evidence-based selection of training compounds for use in the mechanism-based integrated prediction of drug-induced liver injury in man. *Arch. Toxicol.* **2016**, *90*, 2979–3003. [[CrossRef](#)] [[PubMed](#)]
44. James, L.P.; Mayeux, P.R.; Hinson, J.A. Acetaminophen-induced hepatotoxicity. *Drug Metab. Dispos.* **2003**, *31*, 1499–1506. [[CrossRef](#)]
45. Yoon, E.; Babar, A.; Choudhary, M.; Kutner, M.; Pyrsopoulos, N. Acetaminophen-Induced Hepatotoxicity: A Comprehensive Update. *J. Clin. Transl. Hepatol.* **2016**, *4*, 131–142. [[CrossRef](#)] [[PubMed](#)]
46. Court, M.H.; Zhu, Z.; Masse, G.; Duan, S.X.; James, L.P.; Harmatz, J.S.; Greenblatt, D.J. Race, Gender, and Genetic Polymorphism Contribute to Variability in Acetaminophen Pharmacokinetics, Metabolism, and Protein-Adduct Concentrations in Healthy African-American and European-American Volunteers. *J. Pharmacol. Exp. Ther.* **2017**, *362*, 431–440. [[CrossRef](#)] [[PubMed](#)]
47. Kurogi, K.; Rasool, M.I.; Alherz, F.A.; El Daibani, A.A.; Bairam, A.F.; Abunnaja, M.S.; Yasuda, S.; Wilson, L.J.; Hui, Y.; Liu, M. SULT genetic polymorphisms: Physiological, pharmacological and clinical implications. *Expert Opin. Drug Metab. Toxicol.* **2021**, *17*, 767–784. [[CrossRef](#)]
48. Daly, A.K.; Aithal, G.P.; Leathart, J.B.; Swainsbury, R.A.; Dang, T.S.; Day, C.P. Genetic susceptibility to diclofenac-induced hepatotoxicity: Contribution of UGT2B7, CYP2C8, and ABCC2 genotypes. *Gastroenterology* **2007**, *132*, 272–281. [[CrossRef](#)]
49. Ren, Z.; Chen, S.; Pak, S.; Guo, L. A mechanism of perhexiline's cytotoxicity in hepatic cells involves endoplasmic reticulum stress and p38 signaling pathway. *Chem. Biol. Interact.* **2021**, *334*, 109353. [[CrossRef](#)]
50. Sørensen, L.B.; Sørensen, R.N.; Miners, J.O.; Somogyi, A.A.; Grgurinovich, N.; Birkett, D.J. Polymorphic hydroxylation of perhexiline in vitro. *Br. J. Clin. Pharmacol.* **2003**, *55*, 635–638. [[CrossRef](#)]
51. Barclay, M.L.; Sawyers, S.M.; Begg, E.J.; Zhang, M.; Roberts, R.L.; Kennedy, M.A.; Elliott, J.M. Correlation of CYP2D6 genotype with perhexiline phenotypic metabolizer status. *Pharmacogenetics* **2003**, *13*, 627–632. [[CrossRef](#)] [[PubMed](#)]
52. Jaeschke, H. Troglitazone hepatotoxicity: Are we getting closer to understanding idiosyncratic liver injury? *Toxicol. Sci.* **2007**, *97*, 1–3. [[CrossRef](#)] [[PubMed](#)]
53. Hewitt, N.J.; Lloyd, S.; Hayden, M.; Butler, R.; Sakai, Y.; Springer, R.; Fackett, A.; Li, A.P. Correlation between troglitazone cytotoxicity and drug metabolic enzyme activities in cryopreserved human hepatocytes. *Chem. Biol. Interact.* **2002**, *142*, 73–82. [[CrossRef](#)] [[PubMed](#)]
54. Saha, S.; New, L.S.; Ho, H.K.; Chui, W.K.; Chan, E.C.Y. Direct toxicity effects of sulfo-conjugated troglitazone on human hepatocytes. *Toxicol. Lett.* **2010**, *195*, 135–141. [[CrossRef](#)] [[PubMed](#)]
55. Ezhilarasan, D.; Mani, U. Valproic acid induced liver injury: An insight into molecular toxicological mechanism. *Environ. Toxicol. Pharmacol.* **2022**, *95*, 103967. [[CrossRef](#)]
56. Dimitrijevic, D.; Fabian, E.; Nicol, B.; Funk-Weyer, D.; Landsiedel, R. Toward Realistic Dosimetry In Vitro: Determining Effective Concentrations of Test Substances in Cell Culture and Their Prediction by an In Silico Mass Balance Model. *Chem. Res. Toxicol.* **2022**, *35*, 1962–1973. [[CrossRef](#)]
57. Kang, H.K.; Sarsenova, M.; Kim, D.; Kim, M.S.; Lee, J.Y.; Sung, E.; Kook, M.G.; Kim, N.G.; Choi, S.W.; Ogay, V.; et al. Establishing a 3D In Vitro Hepatic Model Mimicking Physiologically Relevant to In Vivo State. *Cells* **2021**, *10*, 1268. [[CrossRef](#)]
58. Correia, C.; Ferreira, A.; Santos, J.; Lapa, R.; Yliperttula, M.; Urtti, A.; Vale, N. New In Vitro-In Silico Approach for the Prediction of In Vivo Performance of Drug Combinations. *Molecules* **2021**, *26*, 4257. [[CrossRef](#)]
59. Di, L. The Impact of Carboxylesterases in Drug Metabolism and Pharmacokinetics. *Curr. Drug Metab.* **2019**, *20*, 91–102. [[CrossRef](#)]
60. Nie, Y.; Yang, J.; Liu, S.; Sun, R.; Chen, H.; Long, N.; Jiang, R.; Gui, C. Genetic polymorphisms of human hepatic OATPs: Functional consequences and effect on drug pharmacokinetics. *Xenobiotica* **2020**, *50*, 297–317. [[CrossRef](#)]
61. Mennecozzi, M.; Landesmann, B.; Palosaari, T.; Harris, G.; Whelan, M. Sex differences in liver toxicity-do female and male human primary hepatocytes react differently to toxicants in vitro? *PLoS ONE* **2015**, *10*, e0122786. [[CrossRef](#)] [[PubMed](#)]
62. Vinken, M.; Hengstler, J.G. Characterization of hepatocyte-based in vitro systems for reliable toxicity testing. *Arch. Toxicol.* **2018**, *92*, 2981–2986. [[CrossRef](#)] [[PubMed](#)]
63. de Bruijn, V.M.P.; Wang, Z.; Bakker, W.; Zheng, W.; Spee, B.; Bouwmeester, H. Hepatic bile acid synthesis and secretion: Comparison of in vitro methods. *Toxicol. Lett.* **2022**, *365*, 46–60. [[CrossRef](#)] [[PubMed](#)]
64. Brecklinghaus, T.; Albrecht, W.; Kappenberg, F.; Duda, J.; Vartak, N.; Edlund, K.; Marchan, R.; Ghallab, A.; Cadenas, C.; Günther, G.; et al. The hepatocyte export carrier inhibition assay improves the separation of hepatotoxic from non-hepatotoxic compounds. *Chem. Biol. Interact.* **2022**, *351*, 109728. [[CrossRef](#)] [[PubMed](#)]
65. Kasteel, E.E.J.; Darney, K.; Kramer, N.I.; Dorne, J.L.C.M.; Lautz, L.S. Human variability in isoform-specific UDP-glucuronosyltransferases: Markers of acute and chronic exposure, polymorphisms and uncertainty factors. *Arch. Toxicol.* **2020**, *94*, 2637–2661. [[CrossRef](#)]
66. den Braver-Sewradj, S.P.; den Braver, M.W.; Baze, A.; Decorde, J.; Fonsi, M.; Bachellier, P.; Vermeulen, N.P.E.; Commandeur, J.N.M.; Richert, L.; Vos, J.C. Direct comparison of UDP-glucuronosyltransferase and cytochrome P450 activities in human liver microsomes, plated and suspended primary human hepatocytes from five liver donors. *Eur. J. Pharm. Sci.* **2017**, *109*, 96–110. [[CrossRef](#)]
67. Driehuis, E.; Kretzschmar, K.; Clevers, H. Establishment of patient-derived cancer organoids for drug-screening applications. *Nat. Protoc.* **2020**, *15*, 3380–3409. [[CrossRef](#)]

68. Boehnke, K.; Iversen, P.W.; Schumacher, D.; Lallena, M.J.; Haro, R.; Amat, J.; Haybaeck, J.; Liebs, S.; Lange, M.; Schäfer, R.; et al. Assay Establishment and Validation of a High-Throughput Screening Platform for Three-Dimensional Patient-Derived Colon Cancer Organoid Cultures. *J. Biomol. Screen.* **2016**, *21*, 931–941. [[CrossRef](#)] [[PubMed](#)]
69. Wang, Z.; Faria, J.; van der Laan, L.J.W.; Penning, L.C.; Masereeuw, R.; Spee, B. Human Cholangiocytes Form a Polarized and Functional Bile Duct on Hollow Fiber Membranes. *Front. Bioeng. Biotechnol.* **2022**, *10*, 868857. [[CrossRef](#)]
70. Bell, C.C.; Lauschke, V.M.; Vorrink, S.U.; Palmgren, H.; Duffin, R.; Andersson, T.B.; Ingelman-Sundberg, M. Transcriptional, Functional, and Mechanistic Comparisons of Stem Cell-Derived Hepatocytes, HepaRG Cells, and Three-Dimensional Human Hepatocyte Spheroids as Predictive In Vitro Systems for Drug-Induced Liver Injury. *Drug Metab. Dispos.* **2017**, *45*, 419–429. [[CrossRef](#)]
71. Leite, S.B.; Wilk-Zasadna, I.; Zaldivar, J.M.; Airola, E.; Reis-Fernandes, M.A.; Mennecozzi, M.; Guguen-Guillouzo, C.; Chesne, C.; Guillou, C.; Alves, P.M.; et al. Three-dimensional HepaRG model as an attractive tool for toxicity testing. *Toxicol. Sci.* **2012**, *130*, 106–116. [[CrossRef](#)] [[PubMed](#)]
72. Gripon, P.; Rumin, S.; Urban, S.; Le Seyec, J.; Glaise, D.; Cannie, I.; Guyomard, C.; Lucas, J.; Trepo, C.; Guguen-Guillouzo, C. Infection of a human hepatoma cell line by hepatitis B virus. *Proc. Natl. Acad. Sci. USA* **2002**, *99*, 15655–15660. [[CrossRef](#)] [[PubMed](#)]

**Disclaimer/Publisher’s Note:** The statements, opinions and data contained in all publications are solely those of the individual author(s) and contributor(s) and not of MDPI and/or the editor(s). MDPI and/or the editor(s) disclaim responsibility for any injury to people or property resulting from any ideas, methods, instructions or products referred to in the content.